

# Color Estimation Error Trade-offs

Ulrich Barnhöfer<sup>\*a</sup>, Jeffrey M. DiCarlo<sup>a</sup>, Ben Olding<sup>c</sup> and Brian A. Wandell<sup>a,b</sup>  
Department of Electrical Engineering<sup>a</sup> and Psychology<sup>b</sup>, Stanford University, Stanford CA, 94305  
<sup>c</sup>Pixim Corporation, Mountain View, CA 94043

## ABSTRACT

Digital imager sensor responses must be transformed to calibrated (human) color representations for display or print reproduction. Errors in these color rendering transformations can arise from a variety of sources, including (a) noise in the acquisition process (including photon noise and sensor noise) and (b) sensor spectral responsivities inconsistent with those of the human cones. These errors can be summarized by the mean deviation and variance of the reproduced values. It is desirable to select a color transformation that produces both low mean deviations and low noise variance. We show that in some conditions there is an inherent trade-off between these two measures: when selecting a color rendering transformation either the mean deviation or the variance (caused by imager noise) can be minimized. We describe this trade-off mathematically, and we describe a methodology for choosing an appropriate transformation for different applications. We illustrate the methodology by applying it to the problem of color filter selection (CMYG vs. RGGB) for digital cameras. We find that under moderate illumination conditions photon noise alone introduces an uncertainty in the estimated CIELAB coordinates on the order of 1-2  $\Delta E$  units for RGGB sensors and in certain cases even higher uncertainty levels for CMYG sensors. If we choose color transformations that equate this variance, the color rendering accuracy of the CMYG and RGGB filters are similar.

**Keywords:** color filter, color conversion, imager sensitivity, digital imager noise

## 1. INTRODUCTION

Successful color reproduction requires the imager to measure enough about the scene spectral composition to make a reasonable prediction of the human color responses to the same scene. The need to estimate the human color responses introduces certain parallels between the imager and the human eye. For example, because the human visual system contains three types of cone photoreceptors, a color camera must make at least three spectral measurements of the scene.

While three samples is a necessary requirement, it is not sufficient. Even when a digital imager makes three spectral measurements, differences in the way the human cone photoreceptors and the digital imager photo detectors sample the spectral signals may cause prediction errors. Most digital imaging pipelines incorporate algorithms designed to minimize the errors caused by converting imager signals into representations designed for human viewing.

While a wide variety of transformations have been discussed in the literature, linear transforms are the most common.<sup>1-4</sup> Linear transformation methods differ mainly in the constraints used to derive the appropriate linear transformation.<sup>5</sup> The main difference between linear methods concerns the selection of signals that are most important for accurate rendering, for example should we emphasize achromatic colors or color saturation? This weighting is sometimes expressed in terms of linear models or databases of likely surfaces and illuminants.

In this paper we focus on the effects of noise in the color imaging pipeline that should be considered in the selection of linear transformations for color rendering. Noise is relevant for all image capture systems because the signal itself is a Poisson process and thus inherently noisy. It is important to choose transformations that minimize the mean color deviation between the estimate and target; it is also important to limit any amplification of the noise present in the signal.

---

\* Correspondence: Email: ulrich@barnhoefer.com, Phone: (650) 725-1255

In some instances, there is a trade-off between minimizing the mean color deviation and minimizing the noise amplification. An example of how these quantities may trade with one another is illustrated in Figure 1. The left hand panel of the figure shows a Gaussian distribution representing the distribution of noisy inputs (i.e., sensor measurements). The right hand panel illustrates two ways these signals can be transformed into the target space (i.e., color signals). One transformation ( $E_1$ ) does a better job matching the mean of the original distribution to the target position (shown as the black square). The mean of the second transformation ( $E_2$ ) is further from the target, but the noise cloud is much smaller.

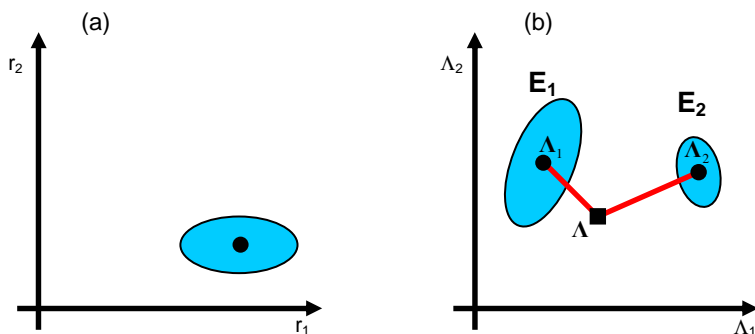


**Figure 1.** Two types of color estimation errors. (a) Noisy (Poisson) sensor data. (b) Linear transformations  $E_1$  and  $E_2$  convert the sensor data into a human calibrated color space. We illustrate two transformations that produce different distributions in the target color space. Transformation  $E_1$  produces a distribution whose mean value is close to the target, but with a large variance. Transformation  $E_2$  produces a distribution whose mean is further from the target, but with a small variance. We describe the implications of these errors for image quality, and we introduce methods for selecting color rendering transformations that minimize a weighted sum of these two types of errors.

In this paper, we describe measurements of the physical noise expected in common digital imaging applications. We then analyze the linear transformations that convert the sensor signals into a perceptual color space (CIELAB). We show how to select linear transformations that trade off the agreement between the target mean and the noise amplification present in the transformation. Then we evaluate these trade-offs for imagers that use two different types of sensors, CMY and RGB.

## 2. COMPUTATIONAL METHODS

We analyze the sensor and digital imaging pipeline in a variety of imaging conditions. The input to the sensor is a spectral photon density chosen based on a typical illuminant (usually D65) and a test surface reflectance (usually drawn from the Macbeth Color Checker). The exposure value (integration time and aperture) is set to a level that produces a few hundred to a few thousand electrons in each pixel; these electron levels are typical of many imaging applications. The calculations described here assume an ideal (noiseless) imager whose only noise is the Poisson noise in the input signal. Hence, the calculations offered here define the upper limits of performance, subject only to inescapable physical noise that can be achieved by any sensor.

### 2.1. Input modeling

The spectral responsivities of the sensor pixels were calculated by assuming a typical photodetector<sup>6,7</sup> and color filter array. The silicon photodetector responsivity is shown in Figure 2a. The pixel responsivities, formed by combining this photodetector with the transmittance of various Brewer Science Pigmented Color Filter Resins RGB and CMY materials,<sup>8</sup> are shown in Figures 2bc. The transmittances were calculated assuming a resin thickness of 1.5 $\mu$ m. Two groups of pigmented resins were selected to simulate a CMY (Figure 2b) and an RGB (Figure 2c) sensor.

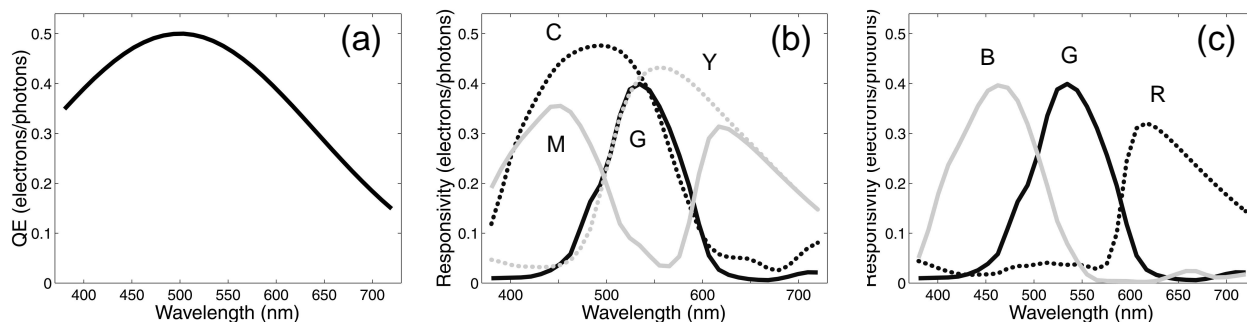


**Figure 2.** The sensor spectral responsivities used for simulations. Panel (a) shows a typical silicon photodetector responsivity.<sup>6,7</sup> Combining the photodetector with CMYG and RGB filters<sup>8</sup> creates a sensor array with CMYG (panel b) or RRGB (panel c) pixels. The simulations further assume a pixel size of  $3\mu\text{m} \times 3\mu\text{m}$  and a 70% fill factor. These values correspond to a typical 4Mpix 1/1.8" CCD sensor.

Figure 3 is an overview of the initial calculation of the noisy photodetector signals. Panel (a) shows the number of photons per  $\text{m}^2/\text{nm}$  (spectral photon distribution) incident at the sensor surface. The other two panels are probability distributions of the pixel electrons for the (b) CMYG and (c) RRGB sensors. The total number of electrons ranges from a few hundred to more than a thousand. The estimated number of electrons is typical for moderate or low illumination conditions, say for an indoor scene. For example, the entire well capacity of a high-resolution imager – say with pixel dimensions of 3 microns on a side – is usually on the order of a few thousand electrons. A signal of about 1000 electrons, shown for the pixels that respond better to the long-wavelength signal, is on the order of a third of the well capacity; a signal of 300 electrons for the less responsive pixels is on the order of a tenth of the well capacity. Such electron counts are observed in many imaging environments and they are quite common in low and medium light imaging environments.

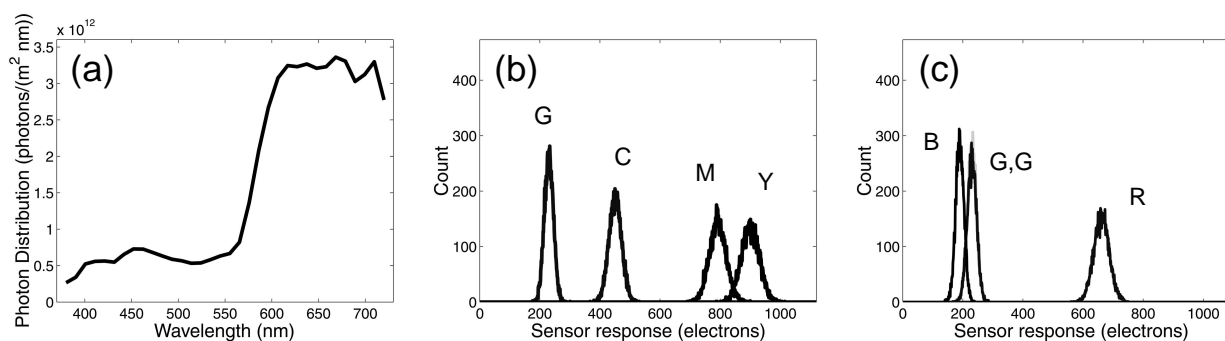


**Figure 3.** Electron generation within the color pixels. (a) Spectral photon distribution of the light incident at the sensor surface from a Macbeth Patch 9, illuminated by a D65 light source. The exposure  $H$  at the sensor surface for the image of a 100% reflector in the same scene was chosen to be  $H_{100\%} = 0.14 \text{ lux}\cdot\text{s}$ . This is equivalent to an ISO400 exposure.<sup>9</sup> The spectral photon signal follows a Poisson noise distribution (not shown). The probability density of electrons within the CMYG and RRGB pixels is shown in panels (b) and (c) respectively.

## 2.2. Choosing the color rendering transformation

The photo-detector electron count variability translates into signal rendering variability at the output of the digital imaging pipeline. We can calculate this output variability in several ways. For example, it is possible to use a computational approach in which we draw a random sample from the photodetector signals and use these random draws

as input to the digital imaging pipeline. The distribution of output values can then be represented in as calibrated human signal in a uniform color space, say, CIELAB.

For the present analysis, we have found it useful to apply an analytic approach. This is possible because in an ideal system the photodetector electron counts are independent Poisson random variables with a fairly high mean. Hence, we can approximate these electron counts as a set of independent Gaussian random variables with different means. Because these Gaussians are approximations to the Poisson, the mean equals the variance.<sup>10</sup>

In the most widely used linear color rendering architecture, sensor signals are linearly transformed into a calibrated color space in preparation for display. We can measure how the noisy signal in the sensor translates into a noisy estimate in a calibrated color space. For the purposes of the calculations in this paper, we describe the errors in CIELAB coordinates. Specifically, suppose there is a color rendering matrix that transforms the sensor responses,  $\mathbf{r}_i$ , into a calibrated space,  $\mathbf{x}_i$ . We then convert these calibrated values into CIELAB values,  $\Lambda_i = (L^*, a^*, b^*) = f(\mathbf{x}_i)$ .

We measure two types of errors for the color rendering transformation. The first error is the difference between the expected and predicted means. Suppose the mean CIELAB value for a test target is  $\Lambda_i$  and the estimated value of this target after the color rendering transformation is  $\hat{\Lambda}_i$ . The CIELAB *bias* is simply the length of the difference,  $\Delta E_i = \|\beta_i\| = \|\hat{\Lambda}_i - \Lambda_i\|$ . For a given color rendering matrix each of the N training patches has its own bias value, and we define the mean bias as

$$\beta_{Lab} = \left( \frac{1}{N} \sum_{i=1}^N \|\beta_i\|^2 \right)^{1/2} \quad (1)$$

In most applications, the best color rendering matrix is chosen by minimizing the mean bias or a similar quantity.

A second type of error measures the effect of the color-rendering matrix on the sensor noise. The uncertainty of the camera measurement (the sensor readings in electrons) propagates through the processing chain into CIELAB-space the following way: a diagonal covariance matrix,  $\Sigma_m$ , represents the independent Gaussian sensor noise variation. The probability density function (PDF) of the sensor error distribution, shown suggestively in Figure 1, is aligned with the sensor axes.

The transformation from xyz to Lab is nonlinear, there is no matrix  $\mathbf{T}$  that describes the coordinate mapping correctly. But the CIELAB formulae are smooth and the transformation from calibrated values,  $\mathbf{x}_i$  to CIELAB values,  $\Lambda_i$ , is well approximated by a local linear transformation,  $\mathbf{T}_i$ , that is derived in the Appendix. Hence, a multivariate Gaussian distribution near  $\mathbf{x}_i$  in sensor space becomes (approximately) a multivariate Gaussian distribution in CIELAB space with covariance matrix  $\Sigma_{Lab_i} = \mathbf{T}_i \Sigma_m \mathbf{T}_i^t$ . We denote a measure of the reproduction noise variance in CIELAB space for the  $i^{\text{th}}$  patch as

$$\gamma_i^2 = \sqrt[3]{|\mathbf{T}_i \Sigma_m \mathbf{T}_i^t|} \quad (2)$$

We prefer estimation matrices that produce a small average reproduction noise. Hence, in addition to the mean bias error, we define a second error term: the average reproduction uncertainty over all patches in the test data set.

$$\gamma_{Lab} = \left( \frac{1}{N} \sum_{i=1}^N \gamma_i^2 \right)^{1/2} \quad (3)$$

Finally, we can choose a color-rendering matrix,  $\mathbf{E}$ , that minimizes a weighted combination of the two error terms,  $\beta_{Lab}^2 + \eta \cdot \gamma_{Lab}^2$ . As the weight  $\eta$  varies the color-rendering matrix minimizes the mean bias ( $\eta = 0$ ) or the reproduction

noise ( $\eta \rightarrow \infty$ ). The calculations in this paper illustrate the effects on image quality for an example set of CMYG and RGGB sensors and a set of surfaces from the Macbeth color checker under a D65 illuminant.

### 3. RESULTS

We compare the CIELAB estimates using CMYG sensors and color rendering transformations subject to minimizing bias or reproduction variance in Figure 4. The transformations minimize the error for the Macbeth color checker surfaces imaged under a D65 illuminant. The figure includes the distribution of estimated CIELAB errors, subject only to sensor photon noise, are shown. The spectral photon distributions of the three test signals are shown in the middle column. The distribution of estimated CIELAB values for a heavy emphasis on minimizing the mean color error is shown in the left column and for a heavy emphasis on minimizing the mean reproduction noise is shown in the right column.

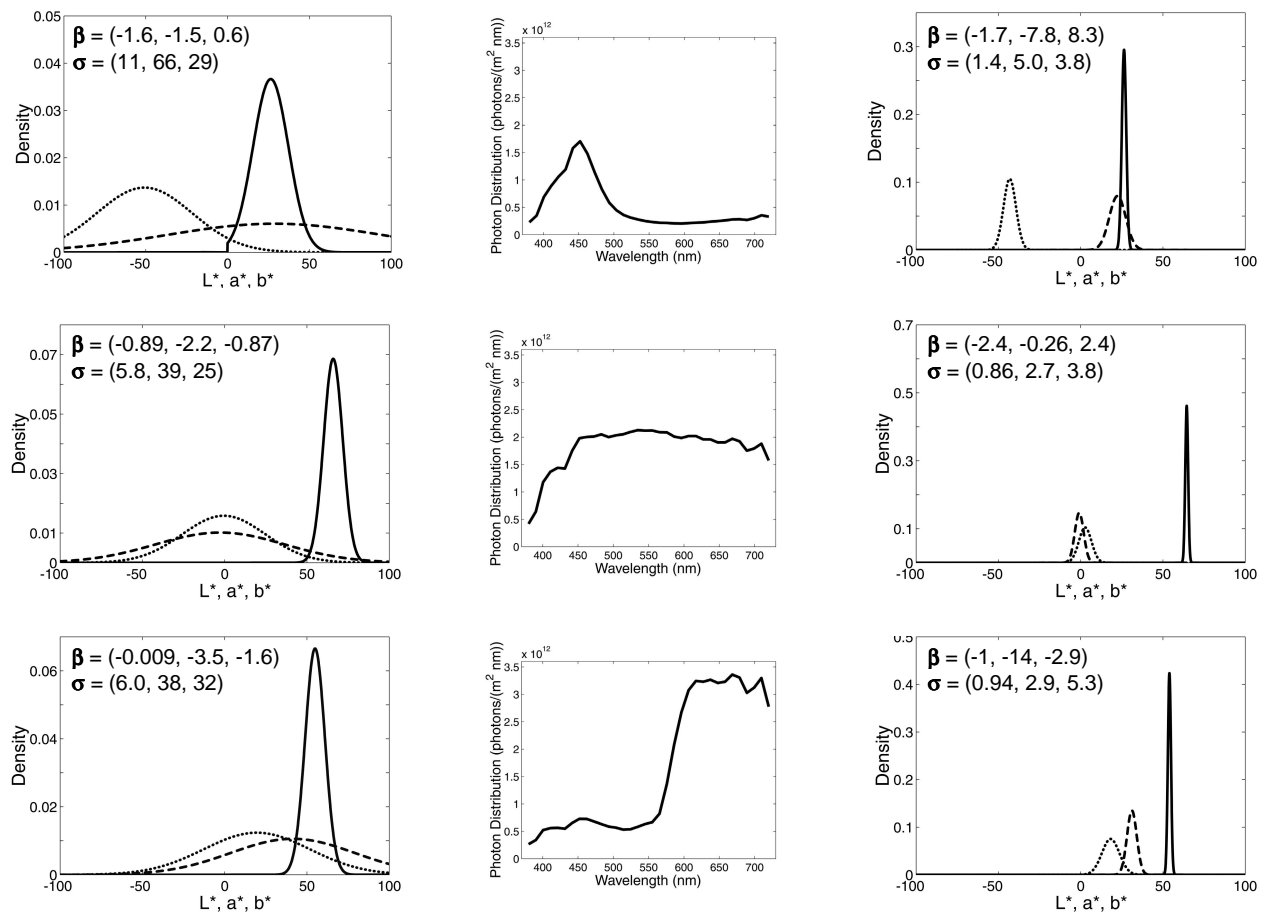
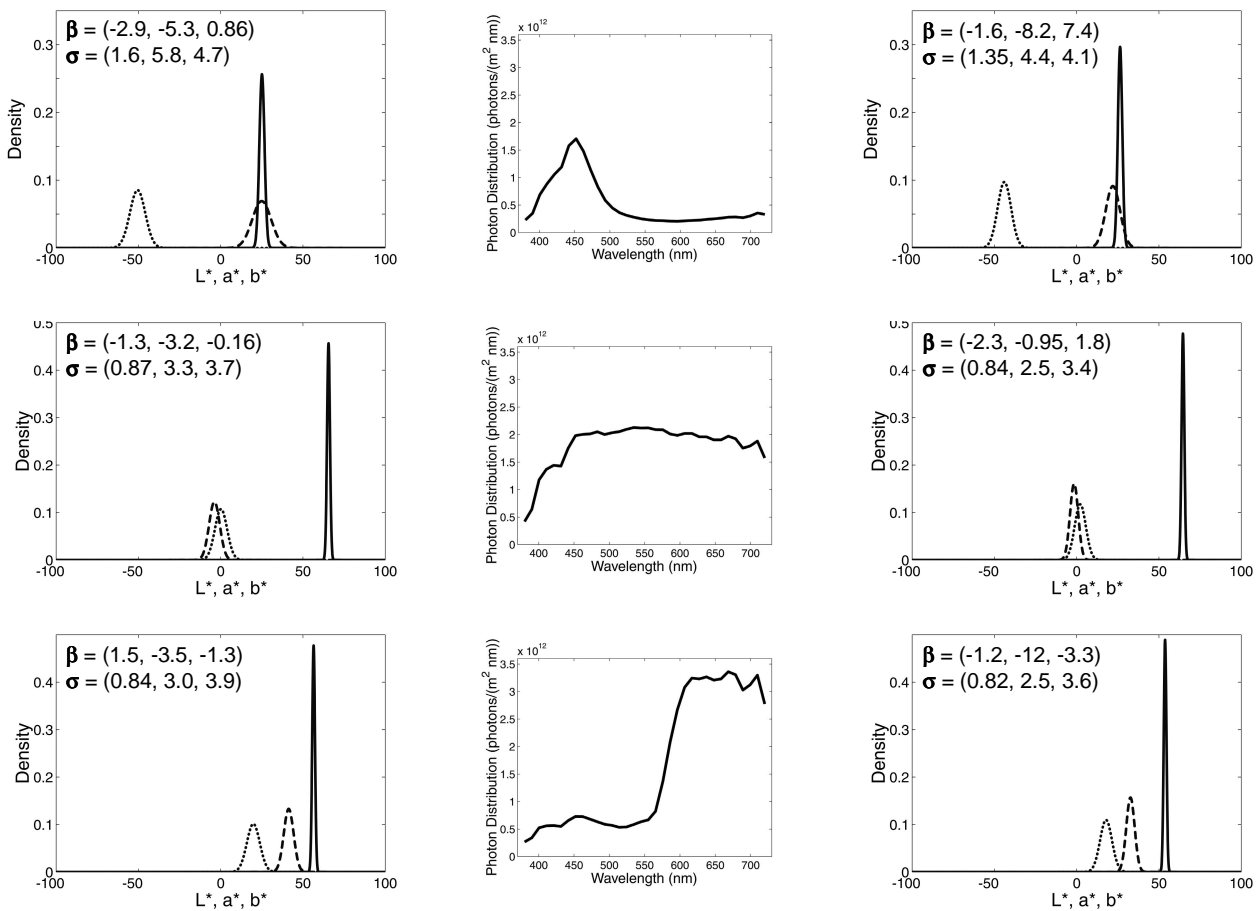


**Figure 4.** Distribution of CIELAB values from a photon-noise limited CMYG sensor. The spectral photon distributions of the three input signals (blue, neutral and red) are shown in the middle column. The distributions of estimated values based on a linear transformation that minimized mainly the mean color error ( $\eta = 0.5$ ) are shown in the left column; distributions for a transformation that minimized mainly the reproduction noise ( $\eta = 100$ ) are shown in the right column. The insets in the panel show the size of the mean bias error and the reproduction variance. Notice that the reproduction variance on the left is very large ( $\sigma_L > 5.8$ ,  $\sigma_a > 38$ ,  $\sigma_b > 25$ ) and it is much smaller on the right ( $\sigma_L < 1.4$ ,  $\sigma_a < 5$ ,  $\sigma_b < 5.3$ ). Estimates are based on signals produced by the twenty-four surfaces of the Macbeth color checker illuminated by a D65 light. In the left and right graphs, the  $L^*$ ,  $a^*$  and  $b^*$  values are shown as solid, dashed and dotted respectively.

Notice that in all cases the physical variation in the electron count produces substantial variance in the CIELAB values. Under moderate to low signal levels, optimizing strongly for the mean bias produces a linear transformation with very poor reproduction variance (left hand graphs). The standard deviation for the  $L^*$  value is more than  $5.8 \Delta E$  units; the standard deviations of  $a^*$  and  $b^*$  estimates are even larger.

Increasing the weight,  $\eta$ , reduces the reproduction noise but increases the bias. In the right hand graphs, the modes of the distributions are shifted away from the true values by a greater amount than in the panels on the left, but the reproduction error for the  $L^*$  value is less than  $1.4 \Delta E$  units (right hand graphs).

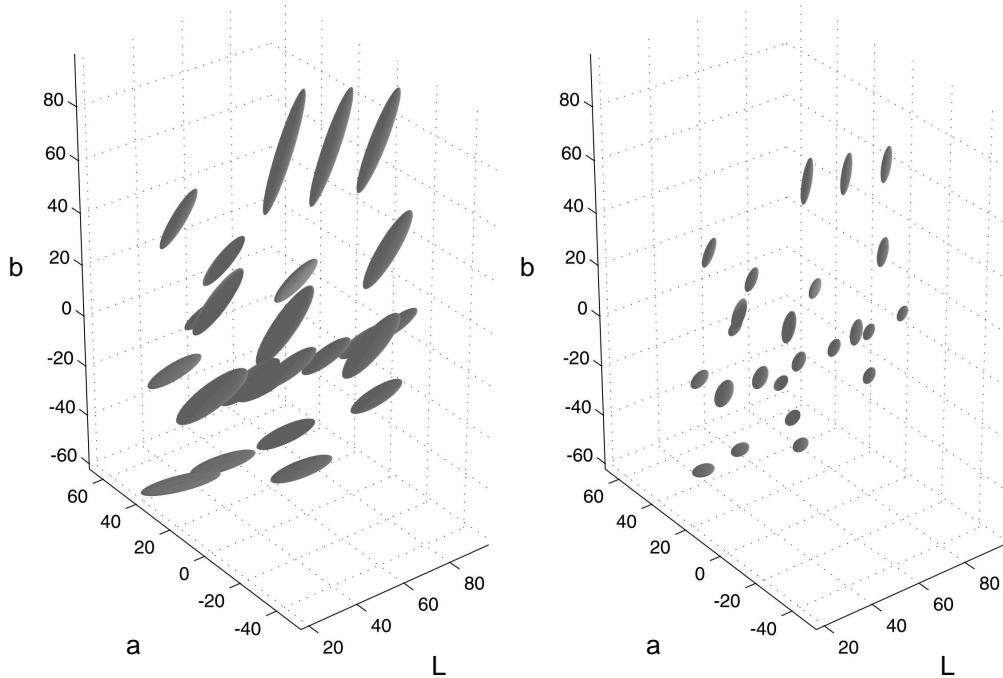
Simulations for the RRGB sensor reveal a different pattern (Figure 5). Varying the weighting between bias and reproduction variance produces improvements in the bias without significant increase in reproduction variance.



**Figure 5.** Distribution of  $L^*$ ,  $a^*$  and  $b^*$  values from a photon-noise limited RRGB sensor. The spectral photon distributions of the three input signals (blue, neutral and red) are shown in the middle column. The distributions of estimated values based on a linear transformation that minimized mainly the mean color error ( $\eta = 0.5$ ) are shown in the left column; distributions for a transformation that minimized mainly the reproduction noise ( $\eta = 100$ ) are shown in the right column. The insets in the panel show the size of the mean bias and the reproduction variance. Unlike the CMYG case (Figure 4), the CIELAB variance is about equal for  $\eta = 0.5$  and  $\eta = 100$ . Other details as in Figure 4.

The data in Figures 4 and 5 do not represent the covariance of the CIELAB errors. This covariance can be described by the ellipsoids representing the level-sets of the probability density functions associated with the CIELAB estimates. The error ellipsoids representing the covariances for the CMYG imager, at two different levels of reproduction noise, are

plotted in Figure 6. The 24 ellipsoids show the error clouds for each of the 24 Macbeth ColorChecker patches. The left hand image shows the result of setting the weight to reduce principally the mean bias; the right hand images shows the effect of minimizing principally the lower reproduction variance.



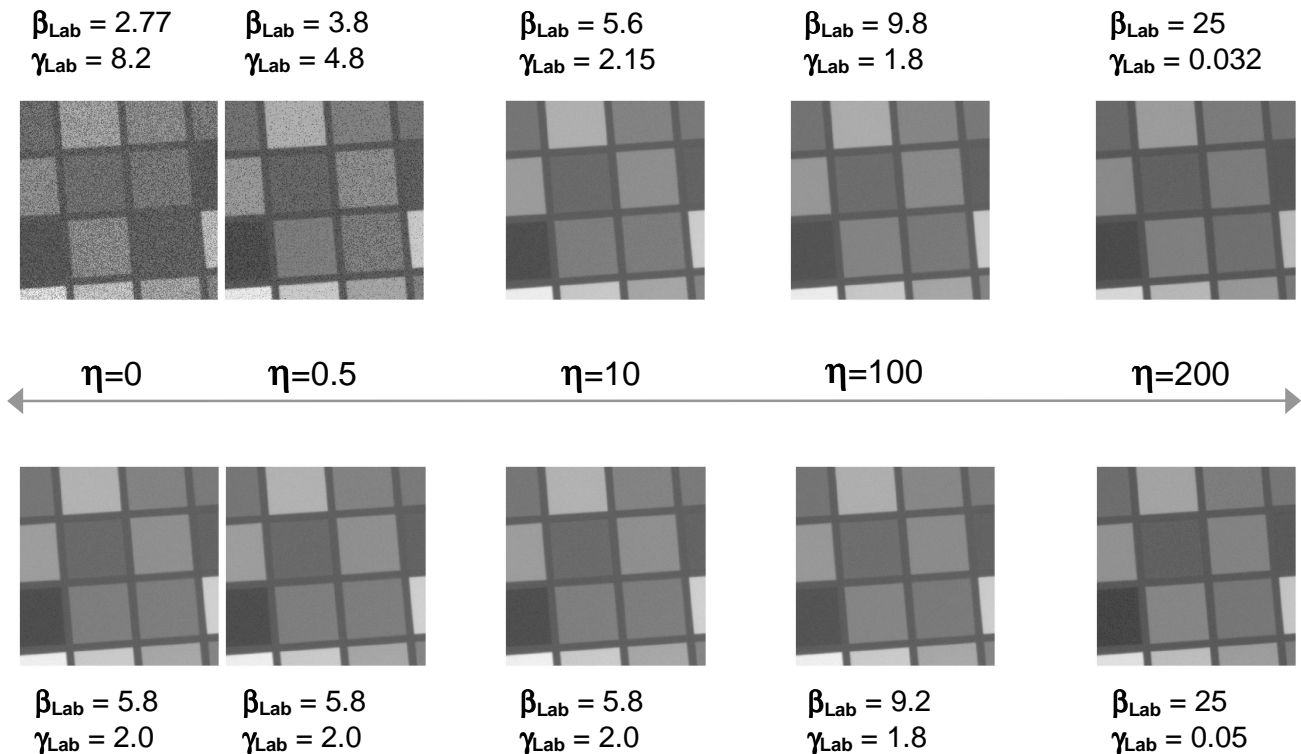
**Figure 6.** Illustration of the noise covariance in  $L^*$ ,  $a^*$ ,  $b^*$  coordinates of the Macbeth color checker estimates using a CMYG sensor. The 24 estimates and corresponding uncertainty ellipsoids for (a)  $\eta = 0.9$ , and (b)  $\eta = 100$ . The mean bias in panel (a) is 4.89 ( $\Delta E$  units) and the mean reproduction uncertainty  $\gamma_{Lab}$  is 3.17. The corresponding values in panel (b) are 9.82 and 1.84. The rendering matrix choice trades off between mean deviation and reproduction variance.

Figure 7 illustrates the effects on image appearance as we shift the emphasis from reducing mean bias to reproduction variance. The images across the rows show the estimated CIELAB images as the selection of linear transform emphasizes mean bias (left) or reproduction variance (right). When using CMYG sensors, the reproduction variance is very salient and appears in the data as spatial noise. As reproduction noise is minimized, the mean bias becomes very large and the image appearance desaturates.

#### 4. DISCUSSION

This paper describes a novel method for selecting color rendering matrices that minimize two types of error: The mean color reproduction error and the reproduction variance. We have used this method to compare CMYG and RGGb color filter arrays. We have tried to understand the error caused by photon noise in a perceptual error space.

We observe several features of the color rendering matrices optimized for CMYG and RGGb sensor types: When matrices were optimized for low reproduction variance, the overall image quality for CMYG and RGGb were very similar. Minimizing for reproduction variance ( $\eta \geq 10$ , see Figure 7) produced very similar reproduction uncertainty  $\gamma_{Lab}$  and bias  $\beta_{Lab}$ . This is a somewhat surprising result because the CMYG filters collect about twice as many electrons under otherwise equal conditions and one might have thought they would have better noise characteristics.



**Figure 7.** Images rendered using transformations selected by varying minimization criteria. The top row shows a sequence of images estimated from a CMYG sensor measurement, the bottom row from an RGGB measurement. The images across each row show the images as the emphasis varies from minimizing mean bias (left) or reproduction variance (right). The images in the upper left show that using a CMYG sensor it is possible to obtain much smaller mean bias at the cost of higher variance. In the RGGB case the smallest mean bias is 5.8, but the reproduction variance does not grow excessively. The simulation conditions are described in the text. The spectral data used for these simulations were obtained by David Brainard.<sup>11</sup>

While color rendering matrices exist that yield a much lower mean bias for the CMYG sensors (2.8  $\Delta E$ ) than for the RGGB array (5.8  $\Delta E$ ), these low values can only be obtained at the price of high reproduction variance (e.g., Figure 7).

A high noise level might be traded for additional accuracy level in high ambient imaging conditions, or for cameras with large pixel sizes (well capacity). But, under moderate illumination conditions photon noise alone introduces an uncertainty in the estimated CIELAB coordinates on the order of 1-2  $\Delta E$  units for RGGB sensors and potentially even higher uncertainty levels for CMYG sensors. This noise is very visible and unattractive. If we choose color transformations that equate the reproduction noise, the color rendering accuracy of the CMYG and RGGB filters are similar.

In an earlier comparison of CMYG and RGB, Baer et al. conclude that the CMYG color rendering is inferior to the RGB color rendering. They also write that the sensitivity of CMYG exceeds that of RGB because ‘three pixels contribute to each super-pixel rather than four, and because the RGB quantum efficiencies are lower (page 21)’.<sup>12</sup> Our analysis differs in several respects. First, we select the color rendering transformations subject to different error norms. Second, we use 2x2 super-pixels (CMYG and RGGB) in both cases.

Baer et al. conclude that the increased quantum efficiency of the CMYG array is canceled by the noise amplifying properties of the color correction matrix. The analysis here generally supports that conclusion.

## 5. CONCLUSIONS

We have analyzed the color rendering transformations used in color reproduction. Specifically, we have analyzed the errors that arise from (a) photon noise in the acquisition process and (b) sensor spectral responsivities inconsistent with those of the human cones. Color rendering transformations can be selected to minimize either the mean color error or the mean reproduction variance (caused by imager noise). We described a methodology for choosing an appropriate transformation for different applications.

We illustrate the methodology by applying it to the problem of color filter selection (CMYG vs. RGGG) for digital cameras. Under moderate illumination conditions photon noise alone introduces an uncertainty in the estimated CIELAB coordinates on the order of 1-2  $\Delta E$  units for RGGG sensors and in certain cases even higher uncertainty levels for CMYG sensors. If we choose color transformations that equate this variance, the color rendering accuracy of the CMYG and RGGG filters are similar.

## 6. ACKNOWLEDGEMENTS

We thank Abbas El Gamal, Hagit Hel-or, Peter Catrysse, Feng Xiao, Xuemei Zhang and Moon Jung Kim for their help and comments on the paper. This work was supported by the members of the Programmable Digital Camera group at Stanford and by a student fellowship from Infineon Technologies to Ulrich Barnhöfer.

## 7. APPENDIX

The goal of the color rendering transformation is to find a transformation that converts the sensor responses  $\mathbf{r}_i = (r_1, r_2, \dots, r_n)_i$  into a calibrated color coordinate frame,  $\mathbf{x}_i$ . In this Appendix we describe how to calculate the mean bias and reproduction variance in CIELAB coordinates for a color rendering transformation,  $\mathbf{E}$ . These analytic methods were used to improve the efficiency of the search routines that minimized the combined bias and reproduction variance.

### 7.1. Notation

$\mathbf{r} = (r_1, r_2, \dots, r_n)$  Sensor responses (measurement-space coordinates)

$\mathbf{X} = (X, Y, Z)$  CIE-XYZ-coordinates

$\mathbf{X}_w = (X_w, Y_w, Z_w)$  The CIE-XYZ white point

$\mathbf{W} = \begin{pmatrix} \frac{1}{X_w} & 0 & 0 \\ 0 & \frac{1}{Y_w} & 0 \\ 0 & 0 & \frac{1}{Z_w} \end{pmatrix}$ , The white-point normalization matrix

$\mathbf{x} = \left( \frac{X}{X_w}, \frac{Y}{Y_w}, \frac{Z}{Z_w} \right)$  Normalized CIE-XYZ-coordinates,  $\mathbf{x} = \mathbf{W}\mathbf{X}$

$\mathbf{E}$  A matrix that relates sensor responses with estimated CIE-XYZ coordinates,  $\mathbf{E}\mathbf{r}_0 = \hat{\mathbf{X}}_0$

$\mathbf{\Lambda} = (L^*, a^*, b^*)$  CIELAB values computed from the normalized CIE-XYZ coordinates

## 7.2. Local CIELAB approximation for calculating the reproduction uncertainty

To specify a color-rendering transformation,  $\mathbf{E}$ , we need to calculate two quantities: The mean bias and the reproduction uncertainty. These quantities are defined in Equations (1) and (3). Were CIELAB-coordinates linearly related to the sensor responses, the minimization would be straightforward. However, the color-rendering transformation only couples sensor responses linearly to CIE-XYZ; the CIELAB coordinates are coupled nonlinearly to CIE-XYZ.

Specifically, for a sensor response  $\mathbf{r}_0$  and its associated estimated normalized CIE-XYZ value,  $\mathbf{WEr}_0 = \hat{\mathbf{x}}_0$ . The CIELAB transformation is

$$\mathbf{\Lambda} = \mathbf{f}(\mathbf{x}) = \begin{pmatrix} 116 & 0 & 0 \\ 0 & 500 & 0 \\ 0 & 0 & -200 \end{pmatrix} \begin{pmatrix} x^{1/3} - \frac{16}{116} \\ x^{1/3} - y^{1/3} \\ z^{1/3} - y^{1/3} \end{pmatrix}$$

For values of  $\mathbf{x}$  near  $\hat{\mathbf{x}}_0$  we can approximate changes in the coordinates of the nonlinear transformation using a linear approximation based on the Jacobian,

$$d\mathbf{\Lambda} = d\mathbf{f}(\hat{\mathbf{x}}_0) = \mathbf{J}(\hat{\mathbf{x}}_0)(\mathbf{x} - \hat{\mathbf{x}}_0)$$

$$\mathbf{J}(\mathbf{x}) = \frac{d\mathbf{f}(\mathbf{x})}{d\mathbf{x}} = \frac{1}{3} \begin{pmatrix} 116 & 0 & 0 \\ 0 & 500 & 0 \\ 0 & 0 & -200 \end{pmatrix} \begin{pmatrix} 0 & y^{-2/3} & 0 \\ x^{-2/3} & -y^{-2/3} & 0 \\ 0 & -y^{-2/3} & z^{-2/3} \end{pmatrix}$$

The local approximation to the transformation from response coordinates to CIELAB coordinates for responses in the neighborhood of the  $i^{\text{th}}$  patch response,  $\mathbf{r}_i + \boldsymbol{\delta}$ , is  $\mathbf{\Lambda}(\mathbf{WEr}_i) + \mathbf{J}(\mathbf{WEr}_i) \mathbf{WE} \cdot \boldsymbol{\delta}$  or  $\mathbf{\Lambda}(\hat{\mathbf{x}}_i) + \mathbf{T}_i \boldsymbol{\delta}$  where

$$\mathbf{T}_i = \mathbf{J}(\mathbf{WEr}_i) \mathbf{WE}$$

The mean bias is calculated using

$$\beta_{Lab} = \left( \frac{1}{N} \sum_{i=1}^N \|\mathbf{\Lambda}(\hat{\mathbf{x}}_i) - \mathbf{\Lambda}(\mathbf{x}_i)\|^2 \right)^{\frac{1}{2}}$$

The reproduction uncertainty, as described in Equations (2) and (3), is calculated using the covariance matrix of  $\mathbf{T}_i$ , namely

$$\Sigma_{Lab_i} = [\mathbf{J}(\mathbf{WEr}_i) \mathbf{WE}] \Sigma_{m_i} [\mathbf{J}(\mathbf{WEr}_i) \mathbf{WE}]^T .$$

## 8. REFERENCES

1. M. J. Vrhel and H. J. Trussell, "Filter considerations in color correction," *SPIE Symposium on Electronic Imaging*, San Jose, CA, 1992.
2. P. L. Vora, J. E. Farrell, J. D. Tietz, and D. H. Brainard, "Linear models for digital cameras.," *IS&T 50th Annual Conference*, 50, 377-382, Cambridge, MA., 1997.
3. F.H. Imai and R.S. Berns, "Spectral estimation using trichromatic digital cameras," *Proceedings of the International Symposium on Multispectral Imaging and Color Reproduction for Digital Archives*, 42-49, 1999.
4. B. A. Wandell, "The synthesis and analysis of color images," *IEEE Transactions on Pattern Analysis and Machine Intelligence*, **PAMI-9**, 2-13, 1987.
5. Jeffrey M. DiCarlo and Brian A. Wandell, "Spectral estimation theory: Beyond linear but before Bayesian," *Journal of the Optical Society of America A*, (in review), 2003.
6. Hamamatsu-Corporation., "Semiconductor Photodetector Arrays," <http://usa.hamamatsu.com/cmp-detectors/arrays/default.htm>, 2003.
7. Sony-Corporation., "CCD Image Sensors," <http://www.sel.sony.com/semi/ccd.html>, 2003.
8. Brewer-Science-Inc., "Specialty Materials Image Sensors," [http://www.brewerscience.com/smproducts/sm\\_image\\_sensor.html](http://www.brewerscience.com/smproducts/sm_image_sensor.html), 2003.
9. ISO12232, "Photography - Electronic still-picture cameras - Determination of ISO speed," 1998.
10. Alberto Leon-Garcia, *Probability and Random Processes for Electrical Engineering*, Addison-Wesley, 1994.
11. D. H. Brainard, "Hyperspectral Image Data," <http://color.psych.ucsb.edu/hyperspectral>, 2000.
12. R. L. Baer, William D. Holland, Jack Holm, and Poorvi Vora, "A comparison of primary and complementary color filters for CCD-based digital photography," *IS&T/SOPIE Conference on Sensors, Cameras and Applications for Digital Photography*, 3650, 16-25, SPIE, San Jose, 1999.